11-1-2020

Effect of Geometry and Fluid Viscosity on Dynamics of Fluid-Filled Cracks: Insights From Analog Experimental Observations

Haitao Cao
Michigan Technological University, haitaoc@mtu.edu

Ezequiel F. Medici
Michigan Technological University, efmedici@mtu.edu

Gregory P. Waite
Michigan Technological University, gpwaite@mtu.edu

Roohollah Askari
Michigan Technological University, raskari@mtu.edu

Recommended Citation

Cao, H., Medici, E. F., Waite, G. P., & Askari, R. (2020). Effect of Geometry and Fluid Viscosity on Dynamics of Fluid-Filled Cracks: Insights From Analog Experimental Observations. *Earth and Space Science, 7*(11). http://doi.org/10.1029/2020EA001333

Earth and Space Science

RESEARCH ARTICLE
10.1029/2020EA001333

Effect of Geometry and Fluid Viscosity on Dynamics of Fluid-Filled Cracks: Insights From Analog Experimental Observations

Haitao Cao[1], Ezequiel F. Medici[2], Gregory P. Waite[1], and Roohollah Askari[1]

[1]Department of Geological and Mining Engineering and Science, Michigan Technological University, Houghton, MI, USA, [2]Department of Mechanical Engineering-Engineering Mechanics, Michigan Technological University, Houghton, MI, USA

Key Points:

- We developed analog physical models by combining high-speed shadowgraph and photoelasticity imaging to study fluid-filled crack dynamics
- Certain geometries result in fluid cavitation and collapse at the crack margin
- The presence of gas at the crack tip may contribute to crack propagation

Correspondence to:
R. Askari,
raskari@mtu.edu

Citation:
Cao, H., Medici, E. F., Waite, G. P., & Askari, R. (2020). Effect of geometry and fluid viscosity on dynamics of fluid-filled cracks: Insights from analog experimental observations. *Earth and Space Science*, *7*, e2020EA001333. https://doi.org/10.1029/2020EA001333

Received 2 JUL 2020
Accepted 23 OCT 2020
Accepted article online 3 NOV 2020

Abstract Fluid-filled volumes in geological systems can change the local stress field in the host rock and may induce brittle deformation as well as crack propagation. Although the mechanisms relating fluid pressure perturbations and seismicity have been widely studied, the fluid-solid interaction inside the crack of a host rock is still not well understood. An analog experimental model of fluid intrusion in cracks between planar layers has been developed to study stress conditions at the margins and tips. A combined high-speed shadowgraph and a photoelasticity imaging system is used to visualize the fluid dynamics and induced stresses on the solid matrix. Cavitation, as well as bubble growth and collapse, occurs along the sawtooth crack margins, which produces a highly localized stress concentration to initiate new subcrack systems. The presence of the bubbles at the crack tip during fluid pressure perturbation can enhance crack propagation.

Plain Language Summary Cracks serve as important fluid pathways in the crust, so their characteristics and density strongly influence fluid flow. At the same time, crack properties are also affected by fluid flow, as their dimensions and connectivity might change under pressures from fluids. Many analytical and experimental studies have been conducted to investigate the effect of subsurface flow on crack dynamics. However, some complexities of crack geometries and fluid properties, in particular when bubbles are present, remain poorly understood. We developed a laboratory analog experiment using an optical imaging system to visualize the induced stresses on a crack. Fluid cavitation and collapse occurring at the margins of a rough crack boundary are observed. In addition, gas bubbles at crack tips significantly contribute to the crack opening. Both observations may help explain crack propagation in underground geological systems.

1. Introduction

Understating the dynamics of magmatic crack growth is crucial for estimating magma transport and eruption precursors. Crack propagation is strongly affected by the stress field caused by the external stress and internal pressure (Sahimi, 2003; Watanabe et al., 2002). Through analytical, numerical, and experimental studies, researchers have evaluated various factors that contribute to the dynamics of crack growth in magmatic systems. Such factors include fluid buoyancy (Weertman, 1971a, 1971b, 1973), reservoir pressure (Lister & Kerr, 1991), magma compressibility (Dahm, 2000), preexisting cracks (Dahi-Taleghani & Olson, 2011; Zhang et al., 2009), fluid viscosity (Heimpel & Olson, 1994), rock heterogeneities (Rivalta et al., 2015), layer rigidities (Kavanagh et al., 2006; Maccaferri et al., 2010; Rivalta et al., 2005), free surface (Rivalta & Dahm, 2006), density gradient (Lister & Kerr, 1991), external stress (Acocella & Tibaldi, 2005; Kervyn et al., 2009; Menand et al., 2010; Watanabe et al., 2002), crack-crack interaction (Ito & Martel, 2002; Takada, 1994), and crack-fault interaction (Le Corvec et al., 2013).

Recently, several studies have been published that investigate volatile bubble expansion as a major force driving magma movement and intrusion (Carey et al., 2012; Chernov et al., 2014; Lyakhovsky et al., 1996; Navon et al., 1998; Nishimura, 2004; Proussevitch & Sahagian, 1998). However, phenomena such as fluid cavitation, which can trigger shock waves to initiate subcracks, are yet to be understood. Cavitation is an important phenomenon, which has been extensively studied in fluid dynamics (e.g., Birkhoff & Zarantonello, 1957; Brennen, 2014; Moholkar & Pandit, 1997; Singhal et al., 2002; Zwart et al., 2004), and

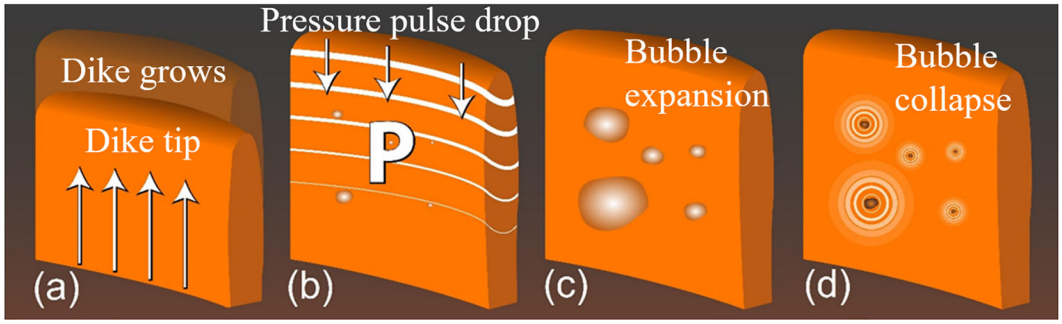

Figure 1. Four stages of cavity collapse in a dike. (a) The magma pushes the rock at the tip of the dike. (b) Once the rock is opened, a pressure pulse drop is initiated at the tip and travels down through the dike. The pressure drop creates small cavity bubbles within the dike. (c) The bubbles continue to grow until reaching their maximum size. (d) They collapse quickly, and shock waves are created.

its damage to pipelines and hydraulic systems has been frequently reported (Tijsseling, 1996). Cavitation occurs when the pressure in the fluid phase suddenly drops below its vapor pressure forming a vapor bubble. As the pressure on the fluid phase returns to the original state, the bubble collapses abruptly and, hence, shock waves are generated. When shock waves reach the solid surface, they can induce high stress that sometimes exceeds the material plastic limit and, thus, cause surface damage. Figure 1 shows a possible process for the generation of cavity bubbles and consequent shock waves during dike propagation. In confined systems like geological cracks or pore spaces, the direction of the dike and sill propagation might be deflected or altered due to the localized stress concentration stemming from the sudden bubble collapse (Joseph, 1995).

Another important aspect of fluid-driven cracks in geological systems that might affect crack propagation is the geometry of the crack and its tip (Desroches et al., 1994; Lenoach, 1995). The shape of the crack tip influences the stress distribution near the tip and the size of the plastic zone. Therefore, the fluid pressure near the tip region in a fluid-filled crack varies with respect to the geometry of the tip. This is particularly important since the stress distribution around the crack strongly depends on the stress condition at the tip, as illustrated in the numerical model of cracks with various geometries, reported by Nilson (1988) and Lecampion et al. (2018). The challenges in modeling fluid-filled cracks include the computational cost and the complexity of mechanisms affecting crack propagation, which makes their mathematical analyses difficult.

In this study, a laboratory analog experiment is developed to study stress conditions at the margins and tips of two-phase fluid-filled cracks in homogeneous and layered media. We show that the geometry of the crack wall and tip contribute to crack growth and that cavitation develops in a crack with rough margins. Our apparatus visualizes fluid flow and stress distribution (stressed area) on crack walls simultaneously. Such visualization at the crack tip and solid-fluid boundary during abrupt stress changes can improve the current understanding of the dynamic of crack propagation.

2. Method

2.1. Experimental Setup

A linear (planar) polariscope is used to visualize the dynamics of the liquid-solid interaction in the filled cracks, subject to a pulse pressure wave originated in the liquid phase; see Figure 2 for more details. The polariscope measures simultaneously the stress wave velocity on the crack wall and visualizes the fluid dynamics. The polariscope can be divided into three parts: a collimated light (also known as shadowgraph system), two linear light polarizers, and a high-speed camera. The light collimation was achieved using a 150 W 21 V halogen light source, followed by a focusing lens with a focal length of 50.8 mm and a diameter of 25.4 mm, a pinhole, and two collimated lenses of focal lengths of 273 and 127 mm, respectively. Two linear polarizers were used to polarize light in a preferred direction, confined to a single plane of oscillation, while all other light oscillation directions are absorbed by the polarizer. When a pair of polarizers are set at orthogonal angle (90°), no light is transmitted through. Some transparent materials, such as polycarbonate, are photoelastic, meaning that when they are under applied stress, they become optically anisotropic (also

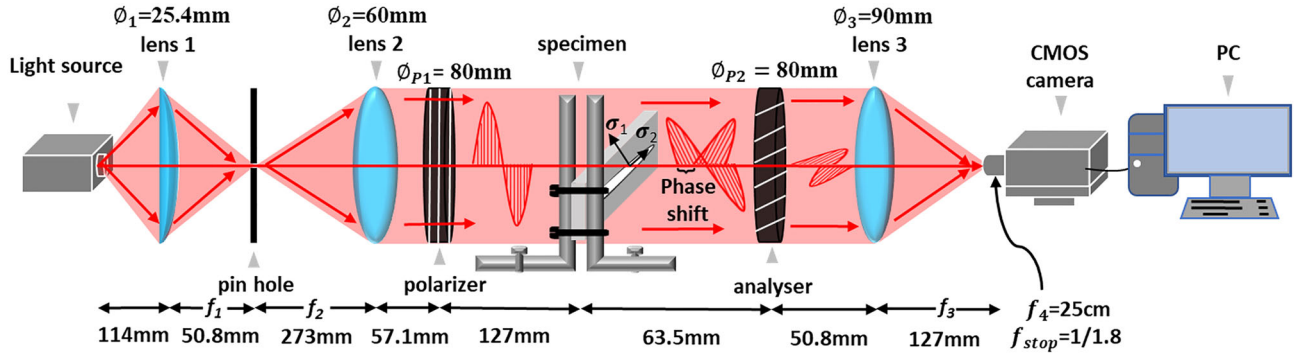

Figure 2. Schematic diagram of the combined high-speed shadowgraph imaging system and linear polarizer setup. The specimen is placed between two steel L-shaped support brackets that are mounted on an optical table. Ø is the lens diameter and *f* the focal length. σ_1 and σ_2 are principal stresses in principal optical axes of the sample.

called birefringent in the literature) and, hence, light is polarized along the two principal stress directions of the sample. The phase shift of the light rays due to the birefringence is proportional to the applied stress (Tada et al., 2000). If we place the photoelastic material between the two orthogonal polarizers, there will be no orthogonally polarized light until the material is stressed, and, thus, we can qualitatively infer the stress level at each point of the sample under load based on the light passing through the system. The fringe envelope that we observe from the linear polariscope is the superposition of the isochromatic and isoclinic fringes. A high-speed camera capable of recording up to 250,000 frames per second (fps) is used to capture the dynamic state of stress in the material, induced by a pressure wave in the liquid phase. In this study we chose to record at 10,000 fps in order to increase the resolution of the individual frames. The high-speed camera was triggered electronically with controlled delay times for taking specific image sequences of the overall fluid motion.

2.2. Analog Crack-Trilayer Model

The experimental apparatus was used to visualize the solid-fluid interactions along the crack main body and at the crack tips in six trilayer models (Table 1), each consisting of two photoelastic insensitive acrylic plates and one photoelastic sensitive polycarbonate plate, as shown in Figure 3a. This trilayer crack model is developed as an analog for the sill intrusion where the liquid intrudes between parallel geological layers. The density of the acrylic is 1,190 kg/m^3, with $V_p = 2{,}710$ m/s and $V_s = 1{,}391$ m/s, while that of the polycarbonate is 1,190 kg/m^3, with $V_p = 2{,}106$ m/s and $V_s = 931$ m/s. The two acrylic layers are $152.4 \times 47.6 \times 1.58$ mm in size, whereas the polycarbonate plate has a dimension of $152.4 \times 47.6 \times 0.79$ mm. The reason we adopt a thinner polycarbonate plate is based on the stress optic law (Tada et al., 2000) stating that thinner photoelastic materials possess higher photoelastic sensitivity, and, thus, smaller external stress is required to generate photoelastic fringes:

$$\sigma = \frac{N f_\sigma}{h} \tag{1}$$

where f_σ is a constant material fringe, N is the fringe order that depends on relative retardation, and h is the specimen's thickness.

The three layers are held together by two 5 mm thick aluminum plates and clamped by bolts along the plates' edges (Figure 3a). Cracks were machined in the middle acrylic layer. The reference crack has flat boundaries (sides) with semicylindrical tips, as shown in Figure 4b, which was used to study solid-fluid interaction and stress propagation on a smooth crack surface. The second crack geometry consists of the same size channel and tips; its boundaries (sides) have, however, a sawtooth pattern where the bottom and height of a triangle is 0.6 and 0.3 cm,

Table 1
Six Experiments to Visualize the Fluid-Filled Crack Dynamics

Experiment	Crack model	Fluid type
1	Flat	water
2	Sawtooth	water
3	Sawtooth	viscous fluid
4	Flat, single narrow tip	water
5	Flat, double narrow tip	water
6	Flat, triangle tip	water

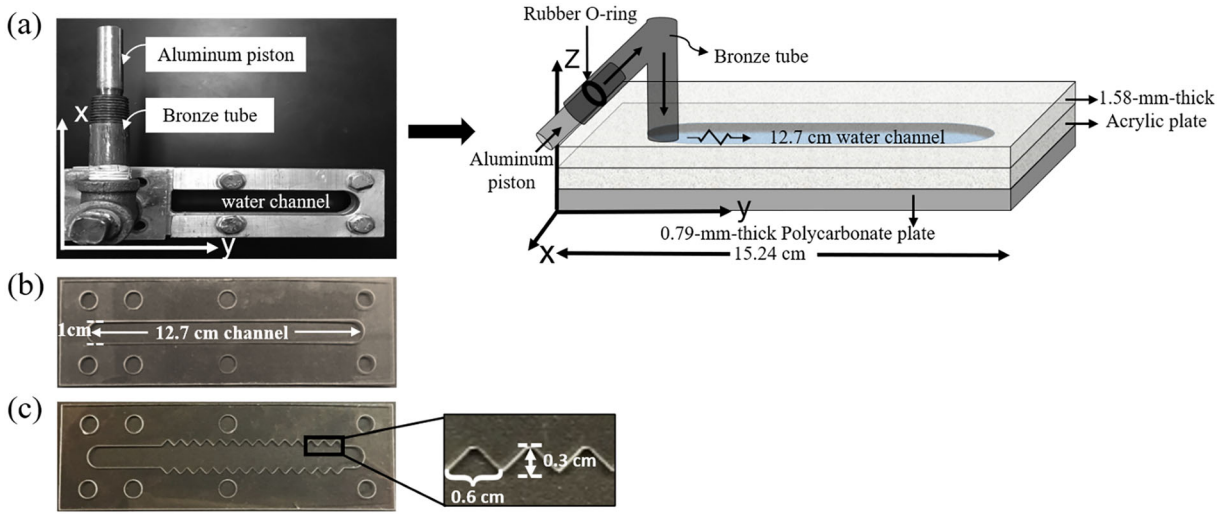

Figure 3. (a) The trilayer model and its schematic view, which consists of one polycarbonate and two acrylic plates, fastened by two aluminum plates. The pressure pulse is produced by applying a sudden load to the aluminum piston. (b) Flat crack model in the middle layer used as a reference. (c) Saw-tooth crack model and enlarged details of its geometry. The circles along the edges of plates are the locations for clamping bolts.

respectively, as shown in Figure 4c. The sawtooth crack wall is common in models of crack morphology that has been used to study crack toughness and fatigue strength (Carpinteri et al., 2019). This sawtooth crack was used as an analog to study the effect of an irregular crack surface on the stress propagation.

Additionally, three types of crack tips were designed to study the fluid-filled crack dynamics in its plastic zone: single narrow tip, double parallel narrow tips, and a triangular tip, as shown in Figures 4a, 3b, and 3c, respectively. The three crack models are also made of acrylic in which the dimensions of the main channels are the same as that of the reference flat crack model. The single narrow and triangle tips shown in Figures 4a and 4c were proposed by Pelloux (1970) and Bowles and Schijve (1983) to study the effect of fatigue in cracks grown for different crack tip geometries. The double narrow tips in Figure 4b were analyzed to study bifurcation performance of a complex crack network in hydraulic fracturing, based on the fractal geometry (Zhou et al., 2017). The analog crack model was filled with distilled water. An experimental test was

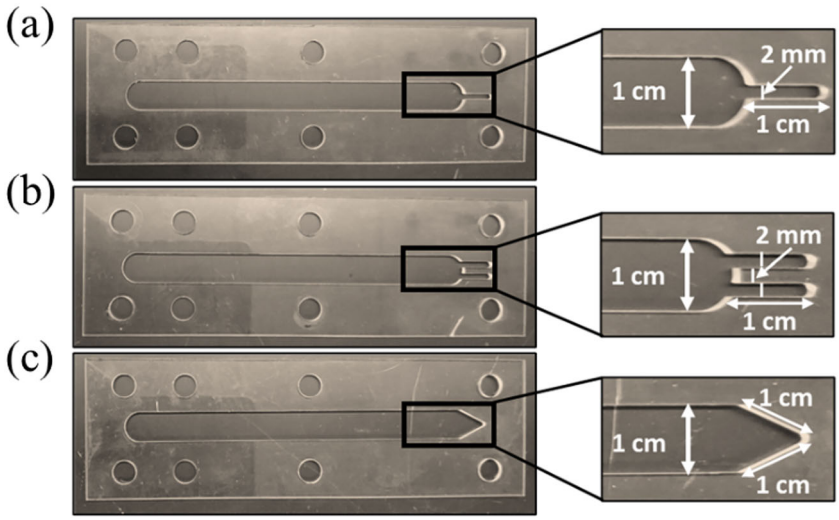

Figure 4. The crack models used to study the fluid-filled crack dynamics in the plastic zone. (a) Single narrow tip with 1 cm length and 2 mm width. (b) Double narrow tips with 1 cm length and 2 mm width each. (c) Triangle tip with 1 cm side length. In crack propagation linear elasticity is valid far from the tip; it breaks down near the tip, where one has a highly nonlinear plastic zone.

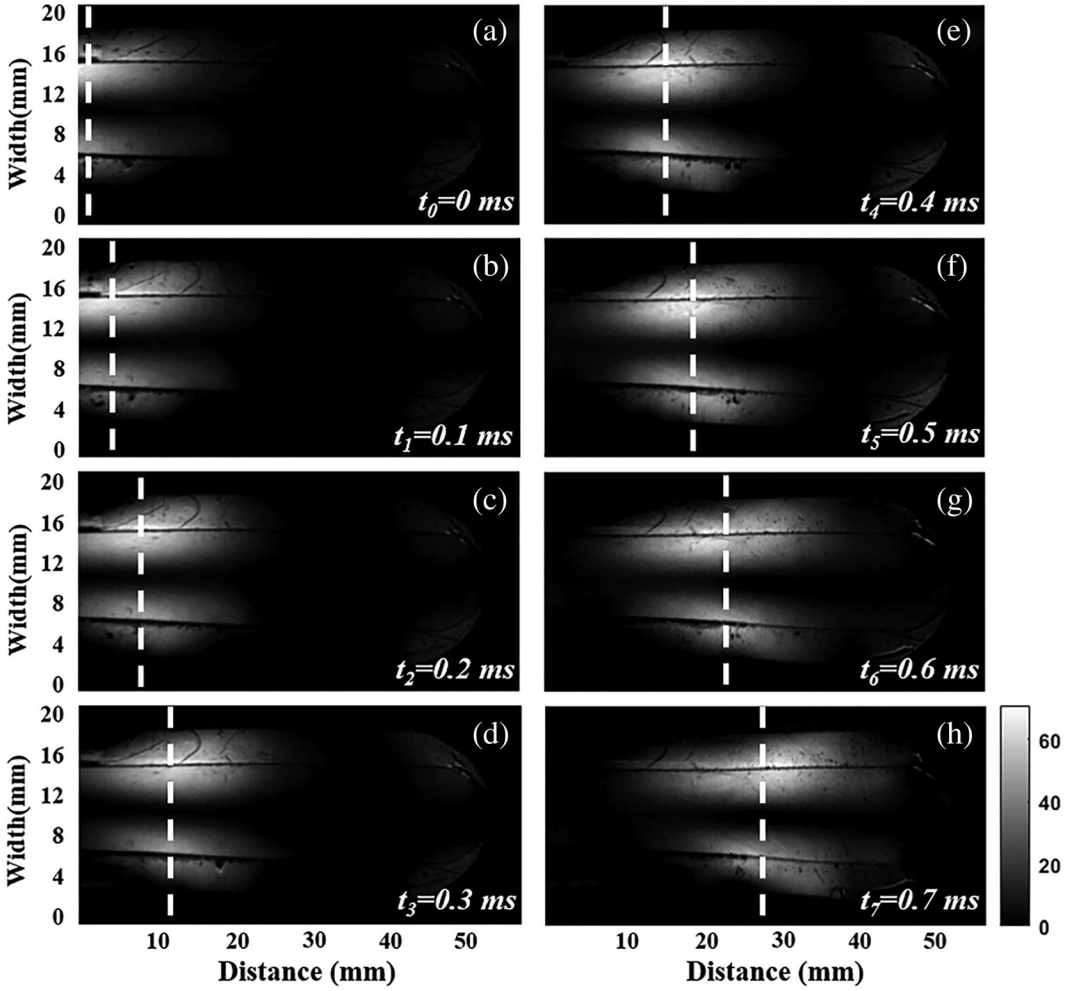

Figure 5. Photoelastic image of the reference smooth flat crack used to show the solid-fluid interaction due to the input pressure pulse on the liquid phase under no surface irregularities. The changing location of the white dashed line represents the direction of the stress wave propagation, which is the result of the photoelastic effect on the polycarbonate layer. The bright patterns near the crack tip are due to the residual stress, caused by clamping bolts. The color bar shows the pixel intensity value of the images. Stressed areas are white, and unstressed areas are black.

initiated by striking the aluminum piston held by a bronze tube, located at one end of the crack in Figure 4a. The impulse on the piston triggers a pressure wave in the liquid phase. The pressure pulse propagates through the confined liquid in the crack and reflects back and forth until it dissipates.

3. Experimental Results

We utilize the reference crack to investigate how the liquid pressure wave is transferred to the solid walls of the crack. The stress wave on the crack walls manifests itself as bright patterns, also known as photoelastic fringes, traveling from one end of the crack to the other along the solid-fluid interface (Figure 5). Due to the limited stress transferred from the stress wave to the polycarbonate plate, the fringe pattern does not manifest as a number of well separated fringes. The velocity of the overall envelope of the stress wave's amplitude (group velocity), measured based on the location of peak pixel intensity of the photoelastic fringes, was 33.95 m/s. Such wave speed in fluid-driven cracks are commonly observed during hydraulic fracturing and in volcanic tremors known as crack waves (Aki et al., 1977; Chouet, 1986; Lipovsky & Dunham, 2015).

In contrast to the idealized smooth crack surface, experiments considering a crack with sawtooth surface representative of crack surface roughness were conducted. The most striking difference between the

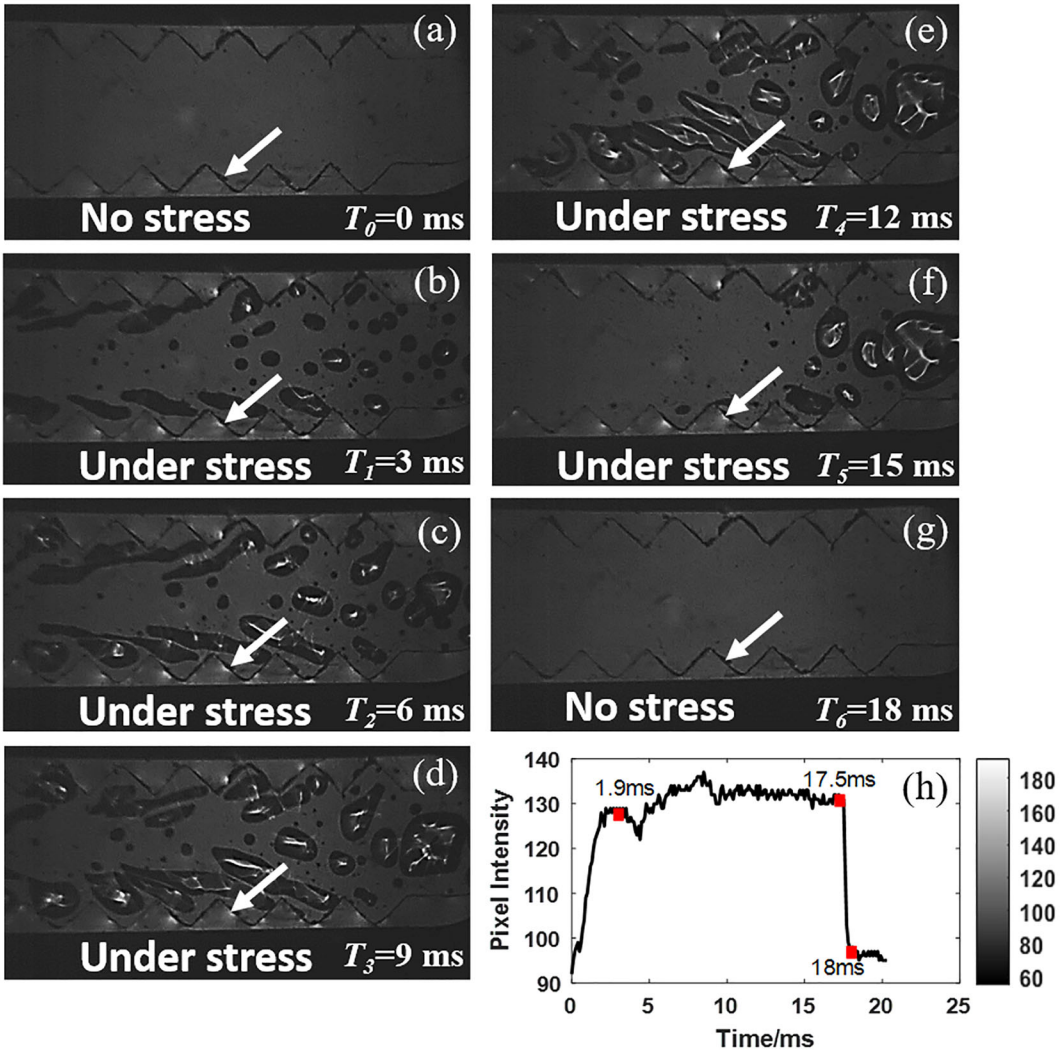

Figure 6. Image sequence of the bubbles expanding and collapsing for the sawtooth crack model. (a) Before the bubble initiation, there is no stress on the sawtooth. (b–f) As the pressure in the liquid decreases, the small-scale bubbles expand, and photoelastic fringes (bright patterns) appear on the crack surface, implying that the crack surface is subjected to a tensile stress due to the bubble expansion. (g) The photoelastic fringes and the associated stress on the crack surface disappear after the pressure in the fluid recovered. (h) The tracked pixel brightness intensity at the sawtooth location indicated by a white arrow in (a–g). This cavitation phenomenon was not observed in the reference crack in Figure 5.

smooth and sawtooth crack models is the appearance of cavitation in the latter (Figures 6a–6g). We repeated this experiment three times, each of which produced the cavitation phenomenon. Figure 6h shows how the pixel values vary at a fixed location in the sawtooth crack indicated by the arrows in Figures 6a–6g during the cavitation process. The pixel values are qualitatively linearly related to the stress (Mindlin, 1939), as a higher pixel value implies greater stress. We observed that before the bubble initiation, there were no photoelastic fringes, meaning no wave-induced stress on the sawtooth. The images in Figure 6 were acquired after the crack wave had decayed so that by 0 ms at T_0 the crack wave-induced strain had diminished. Therefore, the pressure on the liquid decreased and the small-scale bubbles began to expand, photoelastic fringes appeared at the crack surface. This implies that the crack surface is subjected to an intense increase in the tensile stress due to the bubble expansion from 0 to around 1.9 ms. The emergence of cavitation might be due to the shape of the solid-liquid interface and can induce surface self-degradation. The initiation of cavitation bubbles within liquid requires the presence of nuclei that in our system can stem from dissolved gases. As the pressure wave in the liquid phase advances, it reaches a peak value and, then, starts to

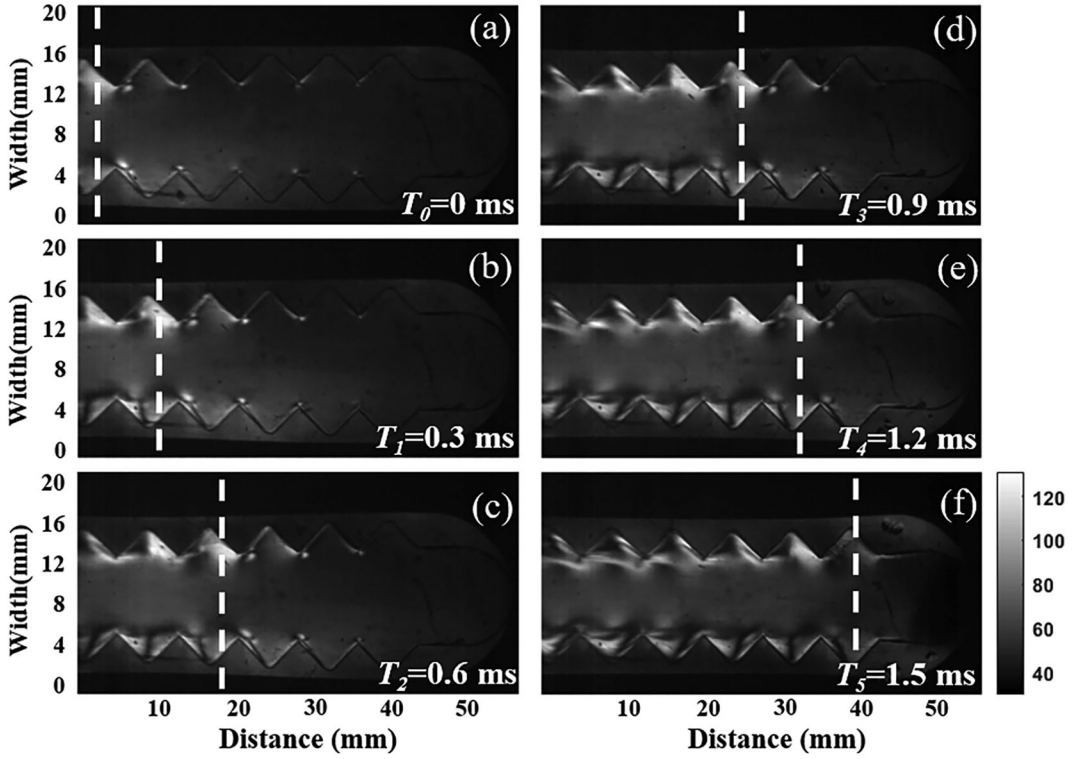

Figure 7. Photoelastic images of the stress wave propagation in the sawtooth crack filled with shampoo. The changing location of the white dashed line represents the direction of the stress wave propagation as in Figure 5. Cavitation phenomenon is not observed in the shampoo filled crack.

decrease. As the pressure decreases below a certain threshold, the microscopic air bubble due to the dissolved gases expand and bubbles emerge. Then, as the pressure induced by the bubble expansion in the liquid increases again, the bubbles collapse violently from around 17.5 to 18 ms, which initiates local shock waves. At the emergence of the bubbles, the stress at the crack surface increases reaching a maximum. This intense stress increases because cavitation at sawtooth crack surface did not develop at the smooth crack's wall. The valley of the sawtooth seems to be of importance to the bubble growth, enhancing the formation of large bubbles and generating a state of stress on the crack wall. During the bubble collapse, on the other hand, the pressure in the fluid recovers, and the associated tensile stress on the crack surface disappears after 18 ms.

To investigate the effect of viscosity on cavitation, we used transparent viscous shampoo (Pantene Pro-V sheer volume) as the crack fluid in the sawtooth crack. Note that the shampoo viscosity is 10^3–10^4 higher than water viscosity (1 mPa·s) at room temperature and pressure (20°C, 101.3 kPa) according to AlQuadeib et al. (2018). Galland et al. (2006) conducted an analog experiment to study the low-viscosity basaltic magma intrusion in crust using vegetable oil whose dynamic viscosity is around 20 mPa·s. Most highly mobile magma should have a viscosity ranging from 4×10^{-6} to 75,000 mPa·s (Galland et al., 2006). Figure 7 shows the stress wave traveling along the sawtooth crack filled with shampoo. The stress wave velocity measured in Figure 7 is 28.3 m/s which is slightly smaller compared to the wave velocity 33.95 m/s in Figure 6 due to the viscous effect. No cavitation is observed because the increase of viscosity enhances the intermolecular forces within the fluid and thus prevents the cavitation (Vernès et al., 2020).

Apart from the expansion and collapse of the bubbles due to the cavitation phenomenon that is likely to produce subcracks along solid boundaries, the bubbles can enhance the opening and propagation of cracks through other mechanisms acting at the crack tip. The stress distribution at the tip of a crack is a key factor for controlling crack propagation. For example, in some deep geothermal systems, it is widely accepted that the crack tip is occupied by magmatic volatiles (Garagash & Detournay, 2000; Rubin, 1993). The typical analytical methods to compute the stress field surrounding the crack tip are based on solving a system of

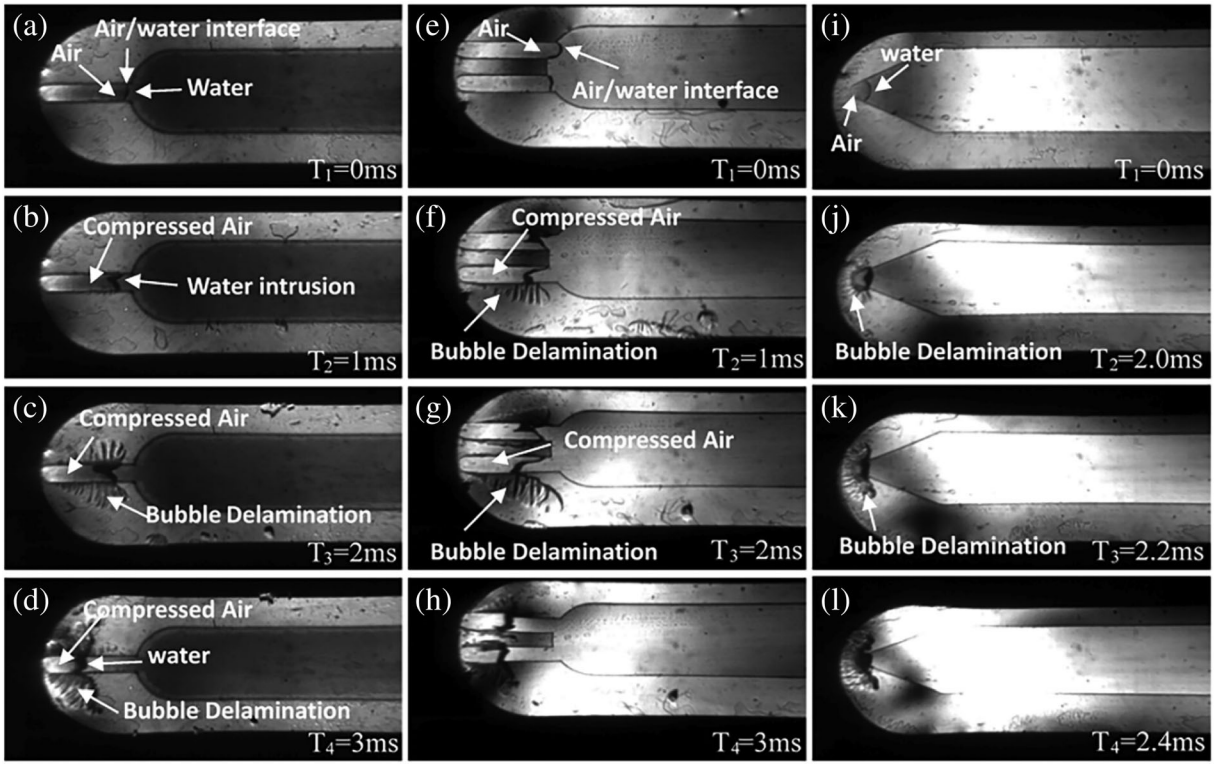

Figure 8. Image sequences showing the process of bubbles emerging at the crack tip. These narrow crack tips were purposely not filled with water to mimic trapped bubbles. The pressure wave in the fluid phase forces the bubble to intrude into the tip, forcing a delamination of the layers of the trilayer model.

coupled equations for the elastic deformation of the host rock and the viscous fluid flow within the crack. However, the behavior of the crack tip is much more complex due to its geometry (Paskin et al., 1985; Zhou et al., 2017).

In order to investigate and visualize the fracturing behavior at the tips for complex geometries when the bubbles are present, the three aforementioned crack models were used, shown in Figures 4a–4c. The tips were purposely not completely filled with water in order to mimic the trapped gas. When the pressure pulse travels through the liquid phase, it compresses and pushes the trapped bubbles forward into the tips. As the bubble pressure increases, the stress on the tip also increases and causes a deformation that resembles a crack opening and the propagation scenario shown in Figure 8. For the single narrow tip in Figures 8a–8d, the pressure wave in the fluid phase forces the bubble to intrude into the tip that creates delamination of the layers of the trilayers model (Figures 8c and 8d). This process is dominated by a wedge-like delamination where the largest opening happens at the gas-fluid interface (Figure 8c). As the liquid pressure keeps pushing and compressing the bubble, the delamination keeps moving forward together with the bubble, leaving behind some smaller bubbles trapped in between the delaminated layers. This is particularly important because if solid particles were present, they could become trapped between the layers, effectively forcing crack expansion and propagation. The double narrow crack tip case shown in Figures 8e–8h shows similar dynamics as the single narrow tip, except that the extent of delamination and, therefore, tip expansion and propagation are significantly enhanced, as indicated by the large lateral opening trailing behind the intruded fluid in Figure 8g.

In the model with the triangular tip, on the other hand, the delamination effect due to the bubble being compressed and pushed by the liquid interface is the least severe of the three cases. This is shown in Figures 8i–8l. We attribute this to two factors related to the bubbles. First, the size of the bubble is smaller than in the previous cases, which leads to a lower compressed volume and smaller stress on the tip bubble-solid interface. Second, the triangular shape induces a gradual compression of the bubble as the meniscus moves forward, as compared with the piston-like compression of the previous two cases, resulting in a maximum compression when the bubble is reduced to the very end of the tip. This gradual compression is then followed by the bubble

bursting of the bubble through the delaminated layers, as seen in Figures 8k and 8l. It is important to note that if the bubbles had not been there, the delamination of the trilayer model representing a crack opening and propagation would not have happened. The gas compression provides the necessary stress concentration to initiate this process.

4. Discussion

Here, we present the effects of the crack wall geometry (i.e., roughness) and crack tip on the mechanics of fluid-filled cracks using analog models. We observed that in a crack with a rough inner surface, bubble cavitation occurs when a transient stress passes through and collapses after an analog injection. The cavitation yields an intense tensile stress on the crack wall. Because shock waves are commonly generated during bubble collapse within a very short time (in the 10^{-6} s time scale), they can potentially provide sufficient energy to create new subcracks (Supponen et al., 2017). Thus, we conclude that not only the state of the stress within the crack but also crack roughness can contribute to crack opening and delamination. The restrictions for capturing the shock waves include the limited number of frames per second (10,000 fps in our experiment) captured by the digital camera, and light source. In other words, a faster digital camera and a stronger light source (laser) that could allow enough light crossing through the sample would be needed for a better resolution of the shock wave.

The crack in the trilayer model is machined in the brittle acrylic plate which is an isotropic and linear elastic material for which typically linear elastic crack mechanics (LEFM) is valid except in the small area in the vicinity of the crack tip (plastic zone). However, the plastic zone size at the tip can be estimated approximately as (Irwin, 1968)

$$R = \left(\frac{1}{2\pi}\right)\left(\frac{K_{IC}}{\sigma_{ys}}\right)^2 \tag{2}$$

where the typical critical stress intensity factor K_{Ic} and yield stress σ_{ys} of acrylic is 1.5 MPa·m$^{0.5}$ (Efimov & Sher, 2001) and 64.8 MPa, respectively, and R is the radial distance ahead of the crack tip.

From Equation 2, the plastic zone radius is 0.08 mm, which is much smaller compared to the size of the crack in our case exhibiting the small-scale yielding at the crack tip; therefore, LEFM is still applicable if no bubble effect occurs at the crack tip as shown in Figure 5. This plastic zone relieves high stress from the fracturing fluid which results in the difficulty in fracturing.

Compared to the crack length, the polycarbonate used in our experiment was thin, implying the plane stress condition. The typical critical stress intensity factor K_{Ic} and yield stress σ_{ys} of polycarbonate is 2.24 MPa·m$^{0.5}$ and 68 MPa, respectively (Williams, 1977). According to Brown and Srawley (1966), the critical thickness T_{c} of polycarbonate plate for plane stress is given by

$$T_{\mathrm{c}} \leq 2.5\left(\frac{K_{\mathrm{Ic}}}{\sigma_{\mathrm{ys}}}\right)^2 \tag{3}$$

Thus, a thickness less than 3 mm is considered as plane stress condition. This explains the discrepancy between our measured crack wave group velocity of 33.95 m/s and the theoretical velocity using the formulation of Lipovsky and Dunham (2015), who assumed an idealized plane strain condition. In addition, the presence of the free surface can partly account for a lower perturbation of the group velocity. Korneev et al. (2014) derived a formula for the velocity of the crack waves from which the velocity of a wave propagating within such a fluid-filled trilayer is lower than that in the plane-strain condition.

Note that the entire clamped trilayer model may be regarded as real cracks in nature of low conductivity or closed cracks. The reopening of the closed crack is by the process of delamination of the tight layers, due to the pressure wave and the presence of bubbles at the crack tip.

5. Conclusions

An analog experimental setup combining two distinct optical techniques, shadowgraphy and photoelasticity, was used to visualize the fluid-solid interaction inside cracks with different types of crack wall surfaces and

tips. Among the most important and striking finding was the occurrence of cavitation when the crack surface wall has a sawtooth shape. This phenomenon can be an important mechanism that leads to the crack growth. The two main causes for the crack surface degradation and growth are, first, the expansion of the bubbles that causes the tensile stress on the crack wall to increase and, second, the collapse of the bubble that generates a shock wave, which was not observed in our experiment because, generally, shock waves occur very fast and, thus, it is impossible to capture this phenomenon using the current setup. We also note that higher fluid viscosity prevents the formation of cavity bubbles. These findings could be used to explain the possibility of cavitation during the magma propagation. If magma has considerable dissolved gases, that is, lower viscosity, it is more susceptible to generating cavity bubbles. On the other hand, for magma with a limited amount of dissolved gases, that is, higher viscosity, cavitation will be less likely.

While we have focused on magmatic systems, the results are also applicable to other fluid-filled crack systems. Fluid injection in hydraulic fracturing and wastewater disposal or fluid intrusion in natural geothermal systems could also form bubbles that consequently open cracks. The bubbles that can be formed could consequently move to crack tips and lead to the formation of new cracks. The same analog experimental setup was used to study the effects of bubbles at the crack tip using various tip geometries. The pressure wave in the liquid phase compresses and pushes forward the trapped bubbles into the tips. The tensile stress induced by the bubbles at the crack tip increase as the bubble pressure increases. The rate of strain energy release at the crack tip increases significantly due to the presence of bubbles, which induce tensile stress. The energy produced by the bubbles overcomes the resistance of the trilayer and results in its delamination, which resembles a crack opening and propagation. The bubble effect plays an important role in crack propagation of fluid-filled cracks and should be incorporated in theoretical models used in studies of crack behavior to supplement linear elastic crack mechanics.

Data Availability Statement

The data and related material of this paper are accessible online (at https://openei.org/datasets/dataset/8aadda44-f712-4f16-a09e-999dc91152fa/resource/d321f63b-b2c6-4735-b8fb-6cde9c10c308/download/data.7z).

References

Acocella, V., & Tibaldi, A. (2005). Dike propagation driven by volcano collapse: A general model tested at Stromboli, Italy. *Geophysical Research Letters*, *32*, L08308. https://doi.org/10.1029/2004GL022248

Aki, K., Fehler, M., & Das, S. (1977). Source mechanism of volcanic tremor: Fluid-driven crack models and their application to the 1963 Kilauea eruption. *Journal of Volcanology and Geothermal Research*, *2*(3), 259–287.

AlQuadeib, B. T., Eltahir, E. K., Banafa, R. A., & Al-Hadhairi, L. A. (2018). Pharmaceutical evaluation of different shampoo brands in local Saudi market. *Saudi pharmaceutical journal*, *26*(1), 98–106. https://doi.org/10.1016/j.jsps.2017.10.006

Birkhoff, G., & Zarantonello, E. H. (1957). *Jets, wakes, and cavities*. New York, NY: Academic Press.

Bowles, C., & Schijve, J. (1983). Crack tip geometry for fatigue cracks grown in air and vacuum. In *Fatigue mechanisms: Advances in quantitative measurement of physical damage* (pp. 400–426). Philadelphia, PA: ASTM International.

Brennen, C. E. (2014). *Cavitation and bubble dynamics*. Cambridge: Cambridge University Press.

Brown, W., & Srawley, J. (1966). Plane strain crack toughness testing of high strength metallic materials. In *Plane strain crack toughness testing of high strength metallic materials* (pp. 1–129). West Conshohocken, PA: ASTM International.

Carey, R. J., Manga, M., Degruyter, W., Swanson, D., Houghton, B., Orr, T., & Patrick, M. (2012). Externally triggered renewed bubble nucleation in basaltic magma: The 12 October 2008 eruption at Halema ʻuma ʻu overlook vent, Kīlauea, Hawaiʻi, USA. *Journal of Geophysical Research*, *117*, B11202. https://doi.org/10.1029/2012JB009496

Carpinteri, A., Spagnoli, A., & Terzano, M. (2019). Crack morphology models for crack toughness and fatigue strength analysis. *Fatigue & Crack of Engineering Materials & Structures*, *42*(9), 1965–1979.

Chernov, A., Kedrinsky, V., & Pil'nik, A. (2014). Kinetics of gas bubble nucleation and growth in magmatic melt at its rapid decompression. *Physics of Fluids*, *26*(11), 116,602.

Chouet, B. (1986). Dynamics of a fluid-driven crack in three dimensions by the finite difference method. *Journal of Geophysical Research*, *91*(B14), 13,967–13,992.

Dahi-Taleghani, A., & Olson, J. E. (2011). Numerical modeling of multistranded-hydraulic-crack propagation: Accounting for the interaction between induced and natural cracks. *SPE Journal*, *16*(03), 575–581.

Dahm, T. (2000). Numerical simulations of the propagation path and the arrest of fluid-filled cracks in the earth. *Geophysical Journal International*, *141*(3), 623–638.

Desroches, J., Detournay, E., Lenoach, B., Papanastasiou, P., Pearson, J. R. A., Thiercelin, M., & Cheng, A. (1994). The crack tip region in hydraulic fracturing. *Proceedings of the Royal Society of London. Series A: Mathematical and Physical Sciences*, *447*(1929), 39–48. https://doi.org/10.1098/rspa.1994.0127

Efimov, V., & Sher, E. (2001). Dynamic crack resistance of acrylic plastic. *Journal of Applied Mechanics and Technical Physics*, *42*(5), 918–924.

Galland, O., Cobbold, P. R., Hallot, E., de Bremond d'Ars, J., & Delavaud, G. (2006). Use of vegetable oil and silica powder for scale modelling of magmatic intrusion in a deforming brittle crust. *Earth and Planetary Science Letters*, *243*(3–4), 786–804.
Garagash, D., & Detournay, E. (2000). The tip region of a fluid-driven crack in an elastic medium. *Journal of Applied Mechanics*, *67*(1), 183–192.
Heimpel, M., & Olson, P. (1994). Buoyancy-driven crack and magma transport through the lithosphere: Models and experiments. In *International geophysics* (Vol. 57, pp. 223–240). San Diego, CA: Elsevier.
Irwin, G. (1968). Linear crack mechanics, crack transition, and crack control. *Engineering Crack Mechanics*, *1*(2), 241–257.
Ito, G., & Martel, S. J. (2002). Focusing of magma in the upper mantle through dike interaction. *Journal of Geophysical Research*, *107*(B10), 2223.
Joseph, D. D. (1995). Cavitation in a flowing liquid. *Physical Review E*, *51*(3), R1649.
Kavanagh, J. L., Menand, T., & Sparks, R. S. J. (2006). An experimental investigation of sill formation and propagation in layered elastic media. *Earth and Planetary Science Letters*, *245*(3–4), 799–813.
Kervyn, M., Ernst, G., van Wyk de Vries, B., Mathieu, L., & Jacobs, P. (2009). Volcano load control on dyke propagation and vent distribution: Insights from analogue modeling. *Journal of Geophysical Research*, *114*, B03401. https://doi.org/10.1029/2008JB005653
Korneev, V., Danilovskaya, L., Nakagawa, S., & Moridis, G. (2014). Krauklis wave in a trilayer. *Geophysics*, *79*(4), L33–L39.
Le Corvec, N., Menand, T., & Lindsay, J. (2013). Interaction of ascending magma with pre-existing crustal cracks in monogenetic basaltic volcanism: An experimental approach. *Journal of Geophysical Research: Solid Earth*, *118*, 968–984. https://doi.org/10.1002/jgrb.50142
Lecampion, B., Bunger, A., & Zhang, X. (2018). Numerical methods for hydraulic crack propagation: A review of recent trends. *Journal of Natural Gas Science and Engineering*, *49*, 66–83.
Lenoach, B. (1995). The crack tip solution for hydraulic fracturing in a permeable solid. *Journal of the Mechanics and Physics of Solids*, *43*(7), 1025–1043.
Lipovsky, B. P., & Dunham, E. M. (2015). Vibrational modes of hydraulic cracks: Inference of crack geometry from resonant frequencies and attenuation. *Journal of Geophysical Research: Solid Earth*, *120*, 1080–1107. https://doi.org/10.1002/2014JB011286
Lister, J. R., & Kerr, R. C. (1991). Fluid-mechanical models of crack propagation and their application to magma transport in dykes. *Journal of Geophysical Research*, *96*(B6), 10,049–10,077.
Lyakhovsky, V., Hurwitz, S., & Navon, O. (1996). Bubble growth in rhyolitic melts: Experimental and numerical investigation. *Bulletin of Volcanology*, *58*(1), 19–32.
Maccaferri, F., Bonafede, M., & Rivalta, E. (2010). A numerical model of dyke propagation in layered elastic media. *Geophysical Journal International*, *180*(3), 1107–1123.
Menand, T., Daniels, K., & Benghiat, P. (2010). Dyke propagation and sill formation in a compressive tectonic environment. *Journal of Geophysical Research*, *115*, B08201. https://doi.org/10.1029/2009JB006791
Mindlin, R. D. (1939). A review of the photoelastic method of stress analysis. *I: Journal of Applied Physics*, *10*, 222–241.
Moholkar, V. S., & Pandit, A. B. (1997). Bubble behavior in hydrodynamic cavitation: Effect of turbulence. *AICHE Journal*, *43*(6), 1641–1648.
Navon, O., Chekhmir, A., & Lyakhovsky, V. (1998). Bubble growth in highly viscous melts: Theory, experiments, and autoexplosivity of dome lavas. *Earth and Planetary Science Letters*, *160*(3–4), 763–776.
Nilson, R. (1988). Similarity solutions for wedge-shaped hydraulic cracks driven into a permeable medium by a constant inlet pressure. *International Journal for Numerical and Analytical Methods in Geomechanics*, *12*(5), 477–495.
Nishimura, T. (2004). Pressure recovery in magma due to bubble growth. *Geophysical Research Letters*, *31*, L12613. https://doi.org/10.1029/2004GL019810
Paskin, A., Massoumzadeh, B., Shukla, K., Sieradzki, K., & Dienes, G. (1985). Effect of atomic crack tip geometry on local stresses. *Acta Metallurgica*, *33*(11), 1987–1996.
Pelloux, R. M. N. (1970). Crack extension by alternating shear. *Engineering Crack Mechanics*, *1*(4), 697–704.
Proussevitch, A., & Sahagian, D. L. (1998). Dynamics and energetics of bubble growth in magmas: Analytical formulation and numerical modeling. *Journal of Geophysical Research*, *103*(B8), 18,223–18,251.
Rivalta, E., Böttinger, M., & Dahm, T. (2005). Buoyancy-driven crack ascent: Experiments in layered gelatine. *Journal of Volcanology and Geothermal Research*, *144*(1–4), 273–285.
Rivalta, E., & Dahm, T. (2006). Acceleration of buoyancy-driven cracks and magmatic dikes beneath the free surface. *Geophysical Journal International*, *166*(3), 1424–1439.
Rivalta, E., Taisne, B., Bunger, A., & Katz, R. (2015). A review of mechanical models of dike propagation: Schools of thought, results and future directions. *Tectonophysics*, *638*, 1–42.
Rubin, A. M. (1993). On the thermal viability of dikes leaving magma chambers. *Geophysical Research Letters*, *20*(4), 257–260.
Sahimi, M. (2003). *Heterogeneous materials: Nonlinear and breakdown properties and atomistic modeling* (Vol. 2): Springer Science & Business Media.
Singhal, A. K., Athavale, M. M., Li, H., & Jiang, Y. (2002). Mathematical basis and validation of the full cavitation model. *Journal of Fluids Engineering*, *124*(3), 617–624.
Supponen, O., Obreschkow, D., Kobel, P., Tinguely, M., Dorsaz, N., & Farhat, M. (2017). Shock waves from nonspherical cavitation bubbles. *Physical Review Fluids*, *2*(9), 093601.
Tada, H., Paris, P., & Irwin, G. (2000). The analysis of cracks handbook. *New York: ASME Press*, *2*, 1.
Takada, A. (1994). Development of a subvolcanic structure by the interaction of liquid-filled cracks. *Journal of Volcanology and Geothermal Research*, *61*(3–4), 207–224.
Tijsseling, A. (1996). Fluid-structure interaction in liquid-filled pipe systems: A review. *Journal of Fluids and Structures*, *10*(2), 109–146.
Vernès, L., Vian, M., & Chemat, F. (2020). Ultrasound and microwave as green tools for solid-liquid extraction. In *Liquid-Phase Extraction* (pp. 355–374): Elsevier.
Watanabe, T., Masuyama, T., Nagaoka, K., & Tahara, T. (2002). Analog experiments on magma-filled cracks. *Earth, Planets and Space*, *54*(12), 1247–1261.
Weertman, J. (1971a). Theory of water-filled crevasses in glaciers applied to vertical magma transport beneath oceanic ridges. *Journal of Geophysical Research*, *76*(5), 1171–1183.
Weertman, J. (1971b). Velocity at which liquid-filled cracks move in the Earth's crust or in glaciers. *Journal of Geophysical Research*, *76*(35), 8544–8553.
Weertman, J. (1973). Can a water-filled crevasse reach the bottom surface of a glacier. *IASH publ*, *95*, 139–145.
Williams, J. (1977). Crack mechanics of polymers. *Polymer Engineering & Science*, *17*(3), 144–149.

Zhang, X., Jeffrey, R. G., & Thiercelin, M. (2009). Mechanics of fluid-driven crack growth in naturally cracked reservoirs with simple network geometries. *Journal of Geophysical Research*, *114*, B12406. https://doi.org/10.1029/2009JB006548

Zhou, Z., Su, Y., Wang, W., & Yan, Y. (2017). Application of the fractal geometry theory on crack network simulation. *Journal of Petroleum Exploration and Production Technology*, *7*(2), 487–496.

Zwart, P. J., Gerber, A. G., & Belamri, T. (2004). *A two-phase flow model for predicting cavitation dynamics.* Paper Presented at the Fifth International Conference on Multiphase Flow, Yokohama, Japan: Fifth International Conference on Multiphase Flow.